Chemical Science

Accepted Manuscript

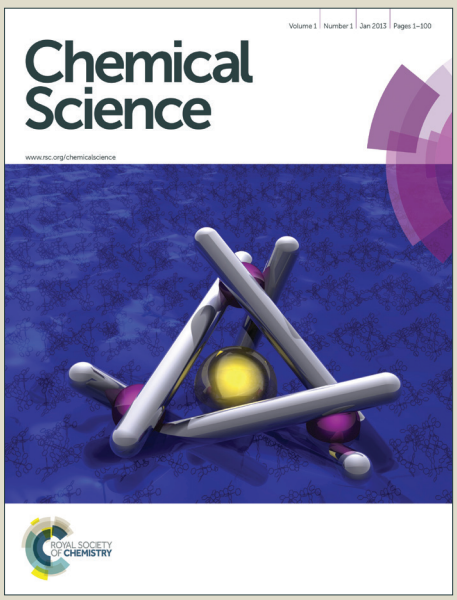

ROYAL SOCIETY OF CHEMISTRY

www.rsc.org/chemicalscience

Cite this: DOI: 10.1039/c0xx00000x

www.rsc.org/xxxxxx

EDGE ARTICLE

Total Synthesis and Characterization of Thielocin B1 as a Protein–Protein Interaction Inhibitor of PAC3 Homodimer

Takayuki Doi,*[a] Masahito Yoshida,[a] Kosuke Ohsawa,[a] Kazuo Shin-ya,[b] Motoki Takagi,[c] Yoshinori Uekusa,[d,e] Takumi Yamaguchi,[d,e] Koichi Kato,[d,e] Takatsugu Hirokawa,[f] and Tohru Natsume[b]

Received (in XXX, XXX) Xth XXXXXXXXX 20XX, Accepted Xth XXXXXXXXX 20XX
DOI: 10.1039/b000000x

We have characterized the inhibition of protein-protein interaction of the homodimer of proteasome assembling chaperone (PAC) 3 with thielocin B1 discovered from natural product sources. Molecular modeling using docking study and molecular dynamics simulation suggested that thielocin B1 exhibits distinct binding poses on the interface of the homodimer and the complex can be stabilized with five interactive residues on PAC3. Thielocin B1 was synthesized for the first time and was utilized for nuclear magnetic resonance (NMR) titration of the PAC3 homodimer. The data revealed significant chemical shift perturbations observed in eight residues on PAC3. We also synthesized a spin-labeled derivative to observe paramagnetic relaxation enhancement (PRE) effects. As a result, distinct decrease of intensities of the NH peaks was observed in sixteen residues of PAC3 in the presence of the spin-labeled derivative. The both NMR experiments and further in silico docking study have suggested that thielocin B1 approaches one face to the PAC3 homodimer not to the monomer, releasing the subunit of the interface of the PAC3 homodimer by a rare pre-dissociation-independent mechanism.

Introduction

Protein–protein interactions (PPIs) play vital roles in numerous cellular functions, e.g., cell growth, DNA replication, and transcriptional activation. PPIs have been considered to be potential therapeutic targets for drug discovery; however, it is difficult to find small-molecule inhibitors that occupy large interaction interfaces of PPIs (750–1,500 A^2).[1] Recent studies have suggested that the protein surfaces are not necessarily flat, but involve grooves or indentations, and consequently, small-molecule inhibitors would not need to cover the entire PPI interface but only interact with high-affinity regions, named "hot spots".[2–4] Another approach is to find small-molecule inhibitors that bind not into the interfaces but to PPI allosteric sites inducing a conformational change of the active site.[5] However, unlike enzymes, for which small-molecules packed in deep pockets have been well-designed, finding potent PPI inhibitors still remains quite a difficult task.[6–8] In addition, there are two possible mechanisms known for inhibition of PPIs: (i) an inhibitor binds to the target protein after dissociation of PPI (pre-dissociation-dependent mechanism), (ii) an inhibitor binds to the proteins inducing dissociation of PPI (pre-dissociation-independent mechanism).[4] The complexity of the mechanisms makes it more difficult to design small-molecule PPI inhibitors. Therefore, it is considered that there is a compelling need for expansion of the screening libraries to find potent PPI inhibitors as the variety of approachable targets has raised up.[9]

In 2009, Shin-ya group has evaluated inhibition of three PPIs, i.e. TCF7/β-catenin, PAC1/PAC2, and PAC3/PAC3, by high-throughput screening of over 100,000 diverse samples of crude metabolites and isolated natural products. Despite a huge chemical space of the natural-product library, the selective hits were found in last two of the three targets and the hit rates were less than 0.01%.[10] Among them, the inhibition of PAC3/PAC3 is of our interest. PAC3, proteasome assembling chaperon 3, identified by Hirano et al. is a component of the α rings of the 20S proteasome.[11] They proposed that PAC3 forms a homodimer, whose crystal structure was elucidated by Yashiroda et al.,[12] associated with the formation of the α ring complexes, together with the PAC1/PAC2 heterodimer,[13] and mediates the correct formation of half-proteasome in cooperation with PAC1/PAC2. PAC3 dissociates before the formation of half proteasomes, and dimerization of the half proteasomes would provide the 20S proteasome. Later, it was reported that a fourth PAC, PAC4 interacts with PAC3 to stabilize each protein. It has been proposed that PAC3 and PAC4 act as a pair in vivo mammalian 20S proteasome assembly;[14–17] therefore, the interaction of PAC3 and PAC4 should be important because siRNA-mediated knockdown[11] of PAC3 and the knockdown[13] of *PAC3* and *PAC4* impaired the proteasome function.

By high-throughput screening of PPI inhibitors from a natural product library as mentioned above, TB1 was found to be a potent and selective PPI inhibitor of the PAC3 homodimer, with an IC_{50} value of 0.020 μM,[10] in addition to JBIR-22 (IC_{50}, 0.2 μM).[20] TB1 was identified as thielocin B1 (**1**), which had been isolated from the fermentation broth of *Thielavia terricola* RF-143 by Yoshida *et al.* as a potent inhibitor for phospholipase A2 (Fig. 1).[18,19] Intriguingly, thielocin A1β and thielocin B3, which have a similar structure to **1**, did not inhibit this PPI. As part of

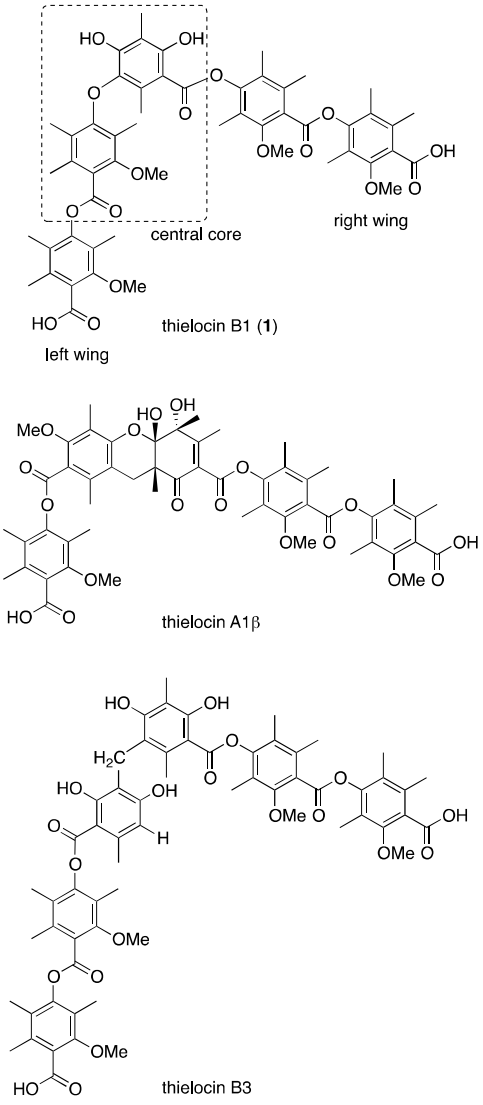

Fig. 1 Structures of naturally occurring thielocins.

our project to characterize PPI inhibitors discovered from a natural product library, we report herein the first total synthesis of **1** and characterization of the inhibition mechanism on the basis of an in silico study of the **1**/PAC3 complex and NMR titration of the PAC3 homodimer with **1** and its spin-labeled derivative.

Results and Discussion

Docking study and molecular dynamics simulation:

Glide docking[21] of thielocin B1 (**1**, active) and thielocin B3 (inactive) was performed by generating various poses on the interface of the PAC3 homodimer (PDB code: 2Z5E).[12] Interestingly, the energetically favored top 100 poses of **1** indicated distinct structures on the surface of β-sheets of PAC3 (Fig. 2a), although no cavities with volumes similar to those of **1** were seen on the interface. On the other hand, the scattered poses of thielocin B3 had lower docking scores than those of **1** (Fig. 2b and 2c). It is conceivable that the central core of **1** defined the angle between the left and right wings; consequently, thielocin B3, which has a different core structure, would not have a suitable shape for binding to PAC3 (See structures in Fig. 1). In

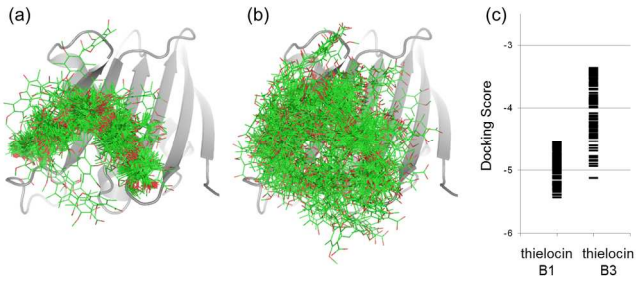

Fig. 2 Overlay of energetically top 100 poses of thielocin B1 (**1**) (carbons in green) (a) and thielocin B3 (b) in the PAC3 dimer interface by docking simulation. (c) Docking score distribution for the complexes of **1**/PAC3 and thielocin B3/PAC3, where 100 poses for each compounds have been retained.

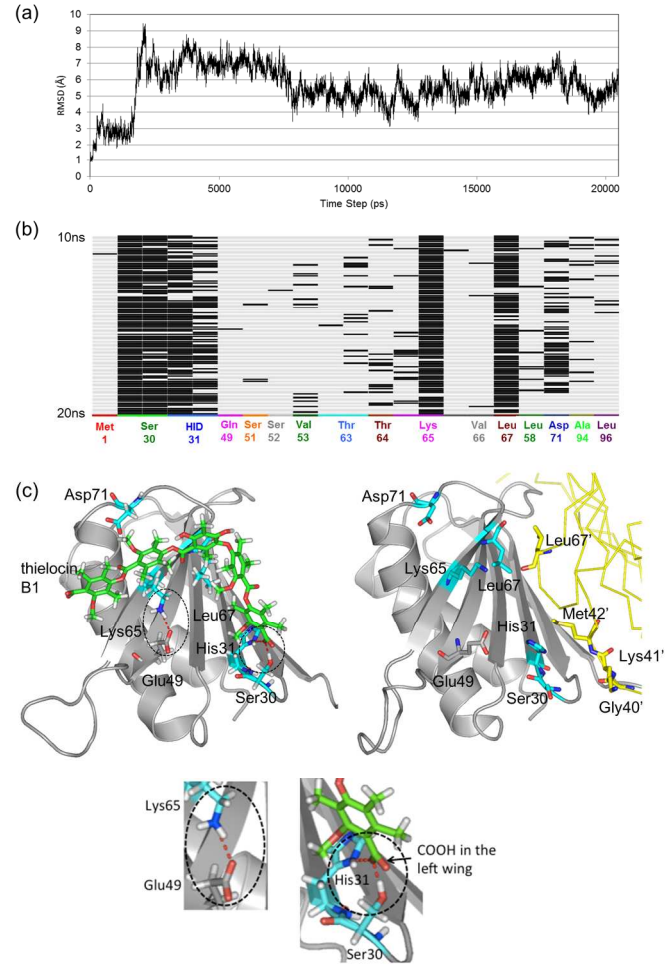

Fig. 3 (a) Root mean square deviation of thielocin B1 (**1**) position to initial docking pose during the 20 ns MD simulation. (b) Barcode view of protein–ligand interaction fingerprint: Met1: Surf, Ser30: ChDon, Surf, His31: ChDon, Surf, Glu49: Surf, Ser51: Surf, Ser52: Surf, Val53: Surf, Thr63: ChDon, Surf, Thr64: Surf, Lys65: ChDon, Surf, Val66: BkDon, Surf, Leu67: Surf, Leu68: Surf, Asp71: Surf, Ala94: Surf, Leu96: Surf. ChDon = sidechain atoms act as H-bond donors. BkDon = backbone atoms act as H-bond donors. Surf = surface contact interactions. (c) A representative structure of **1**/PAC3 complex with five interacting residues (Ser 30, His31, Lys65, Leu67, and Asp71) identified by protein–ligand interaction fingerprint analysis with >40% overall abundance among last 10 ns MD simulation trajectories (left) and the X-ray crystal structure of the PAC3 homodimer (right, PDB code: 2Z5E), in which Ser30–His31/Gly40′–Met42′ and Leu67/Leu67′ are found to be interface.

addition, we performed molecular dynamics (MD) simulation of the top-ranked docking pose of the **1**/PAC3 complex (20 ns) to investigate whether the pose is sufficiently stabilized and which interactions are important for binding. As depicted in Fig. 3a, during MD simulation, the docking pose was quite stable for 20 ns. Protein–ligand interaction fingerprint analysis suggested five interacting residues; Ser30, His31, Lys65, Leu67, and Asp71 on PAC3, with >40% overall abundance among the last 10 ns MD simulation trajectories (Fig. 3b). The representative structure of **1**/PAC3 is illustrated in Fig. 3c (left). Note that Ser30 and His31 that are located in the interface of the PAC3 homodimer by interaction with Gly40′, Lys41′, and Met42′ (Fig. 3c, right), interact with the carboxyl group on the left wing of **1** with high abundance (97% and 86%, sidechain atoms act as H-bond donors; 91% and 61%, surface contact interactions, respectively). The methylenes in Lys65 interact with the dimethylbenzene ring of **1** (96% surface contact interactions), thereby the amino group of Lys65 can intereact with Glu49 by hydrogen bonding (left) although Lys65 locates away from Glu49 in the X-ray crystal structure of the homodimer (right). Leu67 that is also the portion of interface of the homodimer by interaction with Leu67′ (right) would interact with the central core of **1** by surface contact interactions (89%). Asp71 may interact with the methoxy group on the right wing of **1** by surface contact interactions (47%).

Total synthesis of thielocin B1:

To characterize the inhibition mechanism, we planned to study for NMR titration of the complex of PAC3/thielocin B1. However, the supply of **1** from natural sources was limited; therefore, we needed to synthesize **1**. Thielocin B1 (**1**) has a unique structure consisting of a 2,2′,6,6′-tetrasubstituted diaryl ether moiety and 4-hydroxy-2-methoxy-3,5,6-trimethylbenzoic acids by ester linkage. All five benzene rings are fully substituted. Although the syntheses of (+/–)-thielocin A1β,[22,23] thielocin B3,[24] and various derivatives of thielocin B3[25] were reported, none of the thielocins having the 2,2′,6,6′-tetrasubstituted diaryl ether moiety, such as thielocin B1 (**1**), has been synthesized. We envisioned the disconnection of **1** to three units (Scheme 1): central core **2**, left wing **3**, and right wing **4**. The right wing **4** can be synthesized by ester formation between two molecules of benzyl 4-hydroxy-2-methoxy-3,5,6-trimethylbenzoate (**3**). To avoid the significant problem of selective monoesterification of dicarboxylic acid **2a** (Y = CO_2H) with **3** or **4**, we chose monoacid **2b** (Y = H) as a synthetic key intermediate and the introduction of one carboxyl group on the benzene ring after the esterification of **2b** with phenol **4**. Benzyl groups were selected as the protecting groups for phenols and carboxylic acids because hydrogenolysis could remove all benzyl groups in one step under neutral conditions in the final step of the synthesis.

The total synthesis of **1** is illustrated in Scheme 2. Lactone **6** was prepared according to a precedent procedure for alkaline ferricyanide oxidation of **5** utilized in the synthesis of various depsidone derivatives.[26–28] After cleavage of the methyl ether in **6** with BCl_3, both phenolic hydroxy groups were protected with methoxylmethyl chloride (MOMCl). Then, the selective removal of the *ortho*-MOM ether using I_2 in MeOH[29] and protection of the resulting phenol with 4-chlolobenzyl chloride provided **7**.

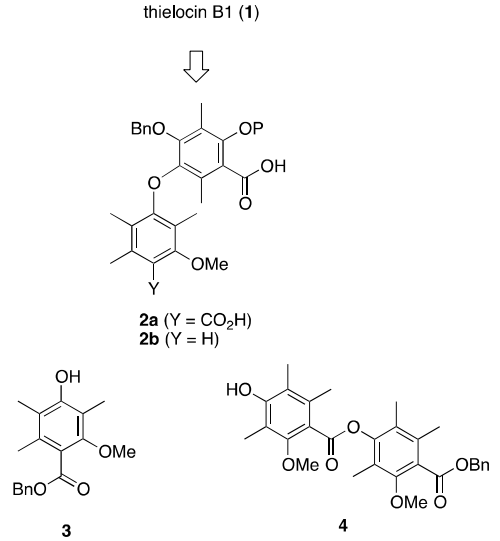

Scheme 1 Retrosynthesis of thielocin B1 (**1**).

Selective reduction of the lactone in **7** with $NaBH_4$ was successfully performed at 0 °C in THF to afford **8** in 66% yield, whereas reduction of the lactone protected with a benzyl ether instead of the 4-Cl benzyl ether resulted in low yield. Electron-withdrawing effect by the 4-Cl atom is crucial for the selective reduction of the lactone in the presence of the methyl ester.[30] Selective benzylation of the resulting phenolic hydroxyl group in **8**, reduction of the benzylic alcohol with Et_3SiH–TFA[31] and removal of the MOM group under acidic conditions in a one-pot reaction, afforded phenol **9**. After the methylation of phenol **9** (MeI, K_2CO_3), basic hydrolysis of the methyl ester **10** was performed at 200 °C under microwave irradiation to afford the central core unit **2b** in 84% yield.[32,33] 2,6-Disubstituents on the benzene ring in **10** would prevent the surrounded methyl ester from hydrolysis under conventional conditions.[34,35] As the core unit **2b** was in our hand, we next investigated the coupling of the right wing **4**.

Esterification of **2b** with the right wing **4**† was performed using 40 equivalent of trifluoroacetic anhydride (TFAA) in toluene at 80 °C to provide **11** in 97% yield.[23,24,36] The reaction was not completed at room temperature. Prior to the formylation of **11**, we conducted a preliminary investigation using **9** and **10**. However, the standard methods, Vilsmeier–Haack,[37] modified Duff,[38] Reimer–Tiemann,[39] and sequential treatment with Br_2/BuLi/DMF, were fruitless. The treatment of **10** with Cl_2CHOMe–$TiCl_4$,[40] resulted in desired formylation in poor yield. Notably, Cl_2CHOMe–AgOTf we recently developed as a potent formylating reagent was quite effective.[41] In fact, rapid formylation of **11** performed at 0 °C led to **12** in 54% overall yield after benzylation of the partially deprotected phenol with 4-chlolobenzyl chloride. Oxidation of aldehyde **12** with $NaClO_2$ in *t*BuOH–H_2O afforded acid **13** (83%).[42] Esterification of **13** with the left wing **3**† using an excess amount of TFAA at 80 °C furnished **14** in 76% yield. Finally, benzyl ether, 4-chlorobenzyl ether, and benzyl esters in **14** were removed by hydrogenolysis (Pd/C 10%, H_2 (1 atm)) in EtOAc–EtOH (1:1) in 15 min. The

Cite this: DOI: 10.1039/c0xx00000x

www.rsc.org/xxxxxx

EDGE ARTICLE

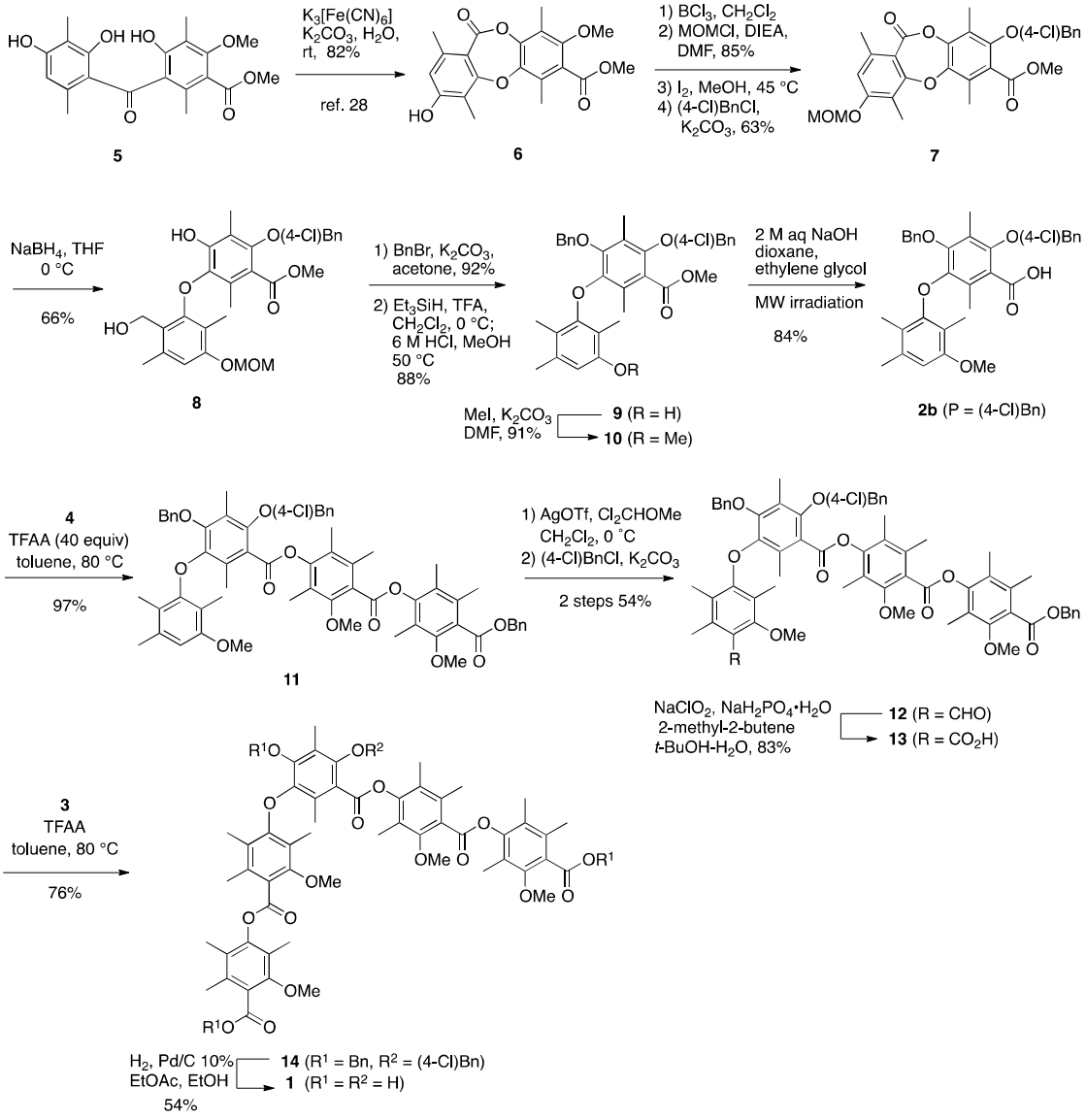

Scheme 2 Total synthesis of thielocin B1 (**1**).

product obtained was immediately worked-up and purified by preparative thin-layer chromatography on silica gel to isolate thielocin B1 (**1**) in 54% yield. The spectral data of the synthetic **1** were in good agreement with those of the natural product. Thus, we accomplished the first total synthesis of thielocin B1 and unambiguously determined its structure.[18]

Inhibitory activity for PPI of the PAC3 homodimer was evaluated using a protein fragment complementation assay with monomeric Kusabira-Green fluorescent protein in vitro, as previously reported.[10,20] The IC_{50} value of synthetic **1** was found to be 0.040 μM, which was in good agreement with that of natural thielocin B1 (0.020 μM).

NMR measurement of the PAC3 homodimer in the presence and absence of thielocin B1:

Next, we undertook NMR experiments in the presence and absence of **1** in hand to elucidate a detailed characterization of PPI inhibition by thielocin B1 (**1**) based on the 3D topological nature of the PAC3 homodimer. Titration of ^{15}N-labeled PAC3 homodimer (0.1 mM) with a 10 mM methanol-d_4 solution of **1** was performed as the final concetractions of **1** were 0.1, 0.2, 0.4, and 0.8 mM, respectively. The progressive spectral changes were

Cite this: DOI: 10.1039/c0xx00000x

www.rsc.org/xxxxxx

EDGE ARTICLE

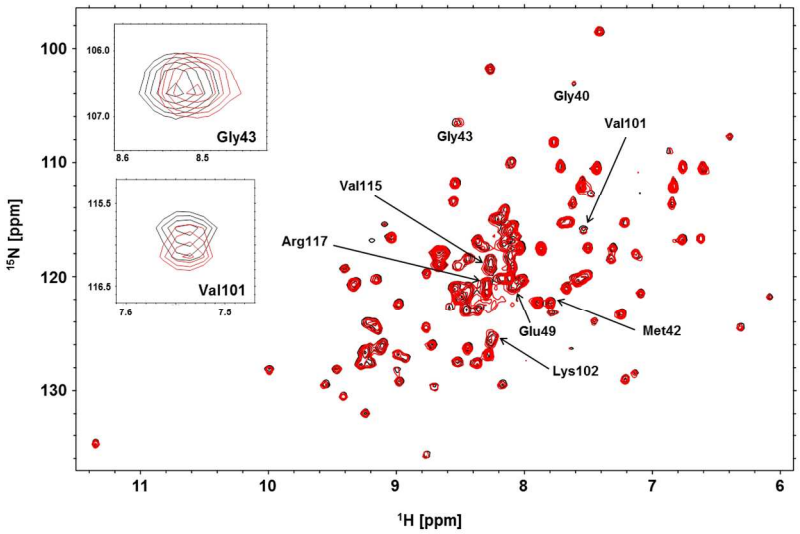

Fig. 4 Superimposed ^{1}H–^{15}N HSQC spectra of the PAC3 homodimer in the absence (black) and presence (red) of four molar excess (to PAC3 protomer) of thielocin B1 (**1**). The peaks showing chemical shift changes $[(\Delta\delta_H)^2 + (0.2\ \Delta\delta_N)^2]^{1/2} > 0.025$ ppm] are labeled in the spectra. As examples, the peaks from Gly43 and Val101 are displayed as insets.

observed as the concentration of **1** increased. Fig. 4 indicates comparison of two ^{1}H–^{15}N HSQC spectra of PAC3 in the presence of four molar excess of **1** (0.8 mM) to the protomer (0.2 mM) and in the absence of **1**. Chemical shift changes were quantified as $[(\Delta\delta_H)^2 + (0.2\ \Delta\delta_N)^2]^{1/2}$, where $\Delta\delta_H$ and $\Delta\delta_N$ are the observed chemical shift changes for ^{1}H and ^{15}N, respectively. The small but distinct chemical shift changes (>0.025 ppm) were induced by **1** for the peaks originating from Gly40, Met42, Gly43, Glu49, Val101, Lys102, Val115, and Arg117 (Fig. 5). As these residues scatter throughout the *monomeric PAC3*, there seems to be no visible relationship between **1** and the *monomeric PAC3*. However, *focusing on the mapped residues on the PAC3 homodimer*[12] (Fig. 5b), we found out that the residues that exhibit distinct chemical shift changes (carbons in magenta) closely related to the interface of the PAC3 homodimer (see Ser30–His31/Gly40′–Met42′ in Fig 3(c), right).

(a)

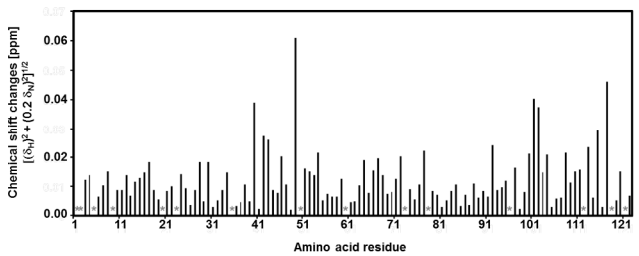

(b)

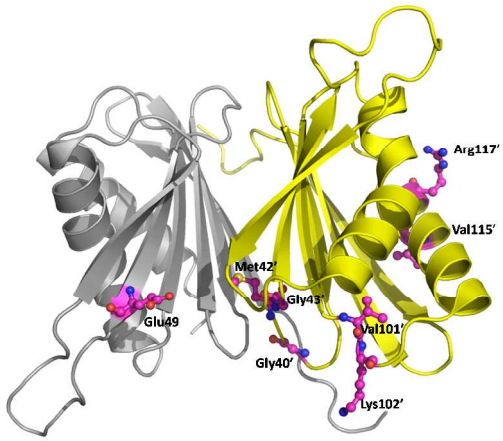

Fig. 5 Chemical shift perturbation of ^{1}H–^{15}N HSQC peaks of ^{15}N-labeled PAC3 (0.2 mM of protomer) upon addition of **1** (0.8 mM). (a) Chemical shift differences are shown according to the equation $\Delta\delta = [(\Delta\delta_H)^2 + (0.2\ \Delta\delta_N)^2]^{1/2}$. Proline residues and the residues whose ^{1}H–^{15}N HSQC peaks could not be used as a probe, because the peaks broadened or were unassigned, are denoted with asterisks. (b) Residues exhibiting distinct chemical shift changes ($[(\Delta\delta_H)^2 + (0.2\ \Delta\delta_N)^2]^{1/2} > 0.025$ ppm), Glu49, Gly40′, Met42′, Gly43′, Val101′, Lys102′, Val115′, and Arg117′, are shown as carbons in magenta (ball and stick model) on the crystal structure of the PAC3 homodimer (PDB code: 2Z5E).

Further titration with **1** resulted in the precipitation of the protein. Presumably, dissociation of the PAC3 homodimer by the binding of **1** would promote aggregation of its destabilized PAC3.

Synthesis of spin-labeled thielocin B1 and PRE effects observation

For additional structual validation, we planned to observe paramagnetic relaxation enhancement (PRE) effects using the spin-labeled derivative of thielocin B1 **15** (Scheme 3). The PRE effects could provide long-distance information because the interaction between a specifically attached paramagnetic nitroxide radical and nearby (<approximately 25 Å) protons causes broadening of their NMR signals due to an increased transverse relaxation rate with an r^{-6} dependence on the unpaired electron–proton distance.[43,44]

The synthesis of spin-labeled derivative **15** is illustrated in Scheme 3. O-Alkylation of phenol **8** with 3-azido-1-iodopropane afforded **16**. Transformation of **16** to **17** was performed according to the method in the preparation of **14** as shown in Scheme 2.† Treatment of **17** with TMSI prepared in situ resulted in removal of the benzyl groups and also substitution of the azido group to iodide, then MOM protection afforded **18** in 55% overall yield. Substitution of iodide **18** with 4-carboxy-2,2,6,6-tetramethylpiperidine 1-oxyl under basic conditions, followed by removal of the MOM groups, and reoxidation of the corresponding *N*-hydroxy derivative formed provided desired nitroxide radical **15** with 90% purity.

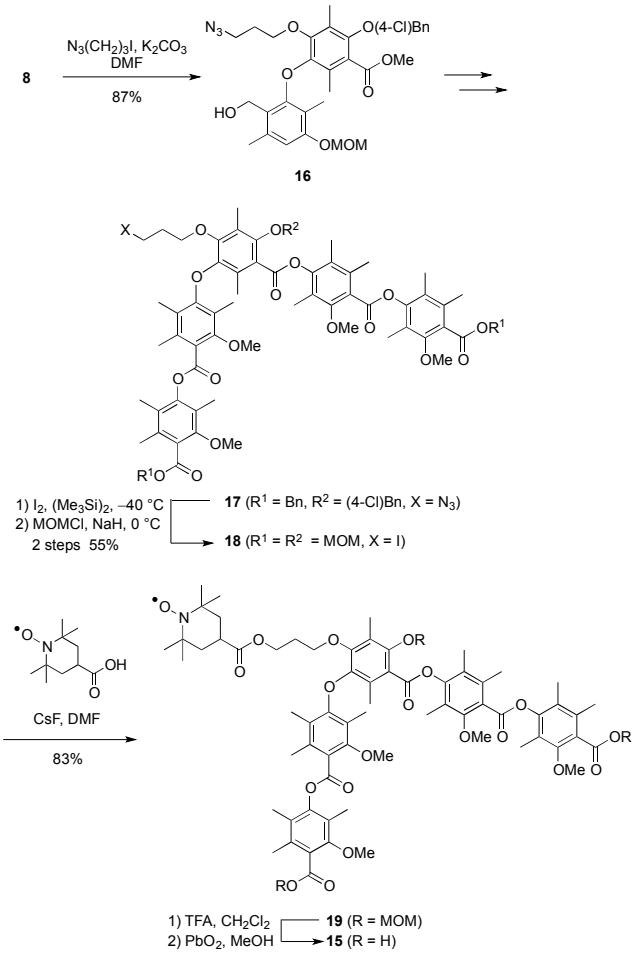

Scheme 3 Synthesis of spin-labeled thielocin B1 **15**.

(a)

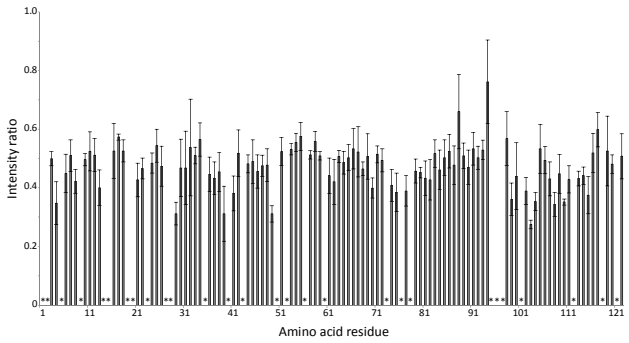

(b)

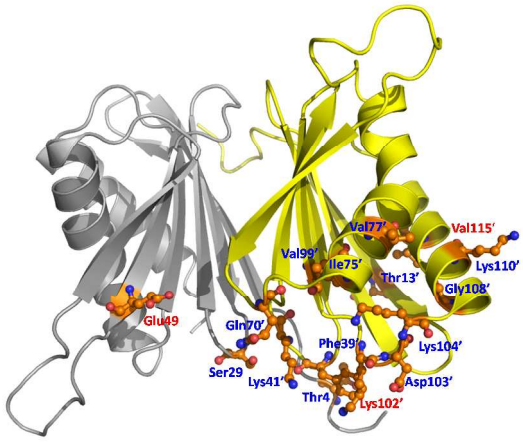

Fig.6 PRE effects observed for $^{1}H–^{15}N$ HSQC peaks of ^{15}N-labeled PAC3 (0.3 mM of protomer) upon addition of spin-labeled **15** (0.9 mM). (a) Plots of the intensity ratios of the NH peaks of PAC3 in the presence of **15** before and after radical quenching with ascorbic acid. Proline residues and the residues whose peaks could not be used as a probe, because the peaks broadened, overlapped, or were unassigned, are denoted with asterisks. Data are mean ± S.D. derived from three separate experiments. (b) The residues exhibiting distinct decrease of peak intensities (< 0.4) Thr4, Ser29, Glu49, Thr13′, Phe39′, Lys41′, Gln70′, Ile75′, Val77′, Val99′, Lys102′, Asp103′, Lys104′, Gly108′, Lys110′, and Val115′ are shown as carbons in orange (ball and stick model) on the crystal structure of the PAC3 homodimer. Both chemical shift changes and weaken intensities were observed at Glu49, Lys102′, and Val115′ labeled in orange.

PRE effects were measured from the peak intensity ratios between two $^{1}H–^{15}N$ HSQC spectra of the PAC3 homodimer (0.3 mM for protomer) acquired in the presence and absence of the nitroxide radical of **15** (0.3, 0.6, 0.9 mM).† When the three equivalent of **15** was added to the PAC3 protomer, distinct decrease of intensities of the NH peaks was observed at Thr4, Thr13, Ser29, Phe39, Lys41, Glu49, Gln70, Ile75, Val77, Val99, Lys102, Asp103, Lys104, Gly108, Lys110, and Val115 residues, respectively (Fig. 6a). The above residues shown as carbons in organge in Fig. 6b are located in certain direction of the PAC3 homodimer. Both chemical shift changes and weaken intensities were observed at Glu49, Lys102, and Val115 resideus. It is conceivable that **15** would approach from the bottom face of the PAC3 homodimer shown in Fig. 6b, and the nitroxide radical moiety in **15** should be close to the right side bottom where most of the residues as shown carbons in orange are mapped.

Docking study for spin-labeled derivative 15 and PAC3 homodimer

Based on the above results obtained by NMR studies, we performed in silico docking study for **15** and the PAC3 homodimer using Molecular Operating Environment (MOE) program.[45] The significant pose obtained is illustrated in Fig. 7a. It suggests that thielocin B1 (**1**) approaches from the bottom face of the PAC3 homodimer shown in Fig. 7a interacting the left wing of **1** with Glu49, closely to the Gly40′–Gly43′ interface of the homodimer. The right wing of **1** is mapped at the left side bottom of the homodimer because the nitroxide moiety in **15** should be close to the right side bottom of the homodimer as the PRE effects were observed. After the approch of **1** to the PAC3 homodimer, it is conceivable that the subunit of interface Gly40′–Gly43′ would be released from Ser30–His31 when the left wing

(a)

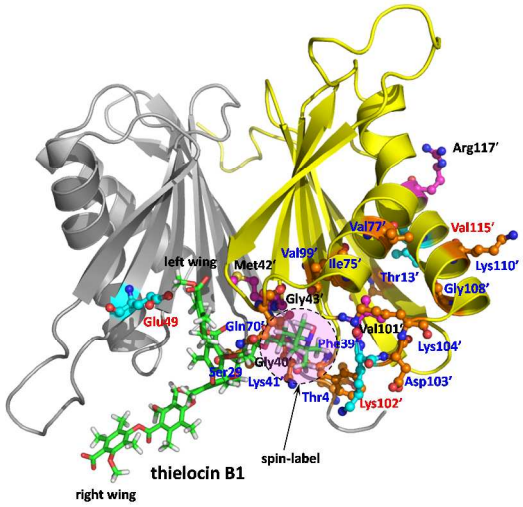

(b)

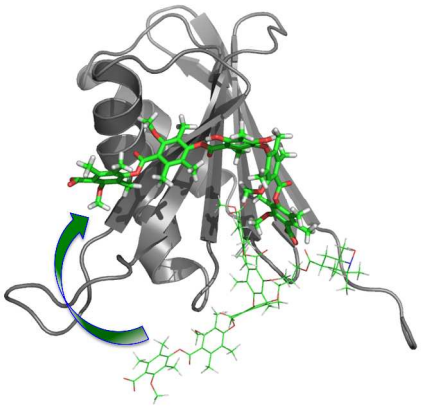

Fig. 7 (a) Docking model of spin-labeled derivative **15** (stick model, carbons in green)/PAC3 homodimer (PDB code: 2Z5E). Residues exhibiting significant chemical shift changes by NMR titration with thielocin B1 (**1**) are shown as carbons in magenta (ball and stick model). Residues exhibiting PRE effects by spin-labeled **15** are shown as carbons in orange. Residues exhibiting both effects are shown as carbons in cyan. (b) Overlay of the MD simulation model of the complex of **1** (stick model)/PAC3 and spin-labeled derivative **15** (wire model) described in the docking model (a)

of **1** may interact to Ser30–His31. Thus, movement of Val101′ and Lys102′ located on the backside of Gly40′–Gly43′ could be induced. It is supported by the fact that the chemical shift changes were observed at Gly40, Met42, Gly43, Val101, and Lys102. The right wing of **1** can move on the β-sheet layers of PAC3 as illustrated in Fig. 7b inducing dissociation of the PAC3 homodimer.

Conclusions

To characterize the inhibition mechanism of thielocin B1 (**1**) discovered from a natural product library as a potent PPI inhibitor of the PAC3 homodimer, we have demonstrated the in silico docking studies of complexes of **1**/PAC3 and thielocin B3/PAC3. It was suggested that distinct structures of **1** on the β-sheets of PAC3 are favored rather than scattered poses observed in the thielocin B3/PAC3 complex with lower docking scores. MD simulation of the top-ranked docking pose of **1**/PAC3 (20 ns) indicated that the complex is considered to be stabilized by the five interacting residues, Ser30, His31, Lys65, Leu67, and Asp71, by sidechain atoms acting as H-bond donors and/or surface contact interactions to **1**.

We also have demonstrated the first total synthesis of thielocin B1. The central core structure, 2,2′,6,6′-tetrasubstitued diphenyl ether **2b**, was synthesized from depsidone derivative **6** via selective reduction of lactone **7**, in which the phenolic hydroxyl group was protected with a 4-chlorobenzyl group. We avoided selective esterification of **2a**; a carboxyl group was introduced after esterification of **2b** with **4**. Efficient formylation of **11** using Cl_2CHOMe–AgOTf was performed to afford **12**. Oxidation of the aldehyde **12**, esterification of the resulting acid with **3**, and hydrogenolysis furnished thielocin B1 (**1**) whose spectral data were identical to those of the natural product. Therefore, the structure of **1** was unambiguously determined. Synthetic **1** exhibited potent inhibitory activity for PPI of the PAC3 homodimer, with IC_{50} value of 0.040 μM, which was in good agreement with that of natural thielocin B1 (0.020 μM).

The NMR titration experiment of the PAC3 homodimer (0.2 mM for protomer) with **1** (0.8 mM) indicated distinct chemical shift changes at Gly40, Met42, Gly43, Glu49, Val101, Lys102, Val115, and Arg117. These results suggest that **1** intercalates into the PAC3 homodimer rather than monomeric PAC3. However, further titration with **1** failed due to precipiation of the protein. For further structual validation, spin-labeled **15** was synthesized, and PRE effects for the PAC3 homodimer were measured in the presence and absence of nitroxide radical of **15**. PRE effects were observed at Thr4, Thr13, Ser29, Phe39, Lys41, Glu49, Gln70, Ile75, Val77, Val99, Lys102, Asp103, Lys104, Gly108, Lys110, and Val115 residues when the three equivalent of **15** was added to the PAC3 homodimer (0.3 mM for protomer). Based on the results of above NMR studies and additional docking study for spin-labeled derivative **15** and PAC3 homodimer, we conclude thielocin B1 (**1**) approaches from the bottom face of the PAC3 homodimer as shown in Fig. 7a interacting the left wing of **1** with Glu49, closely to the Gly40′–Gly43′ interface of the homodimer. The right wing of **1** is mapped at the left side bottom of the homodimer because the nitroxide radical moiety in **15** should be close to the right side bottom of the homodimer as the PRE effects were observed. Then, the subunit of interface Gly40′–Gly43′ would be released from Ser30–His31 when the left wing of **1** may interact to Ser30–His31 as the chemical shift changes

were observed at Val101′ and Lys102′ located on the backside of Gly40′–Gly43′ as well as at Gly40′, Met42′, and Gly43′. The fact that PAC3 was precipitated in the presence of more than four molar excess of **1** to the protomer indicates that the dissociation of the homodimer by the intercalation of **1** would destabilize the structure of PAC3 in an aqueous solution.

The overall results suggest a roof-like binding pose of the complex of **1**/PAC3 similar to the crystal structure of the complex of ZipA with an inhibitor, as reported previously.[46] The hypothesis that PPI inhibitors contain small scaffolds with multiple aromatic rings connected by rigid linkers[47] is highly matched in our results. The results also suggest that thielocin B1 promotes PPI inhibition of the PAC3 homodimer by a rare pre-dissociation-independent mechanism, such that a small molecule can intercalate into the dynamic trimer complex of TNF,[48] or surviving homodimers.[49] We think our approach to the discovery of natural-product-based PPI inhibitors confirms the likelihood of finding a highly potent and selective inhibitor. Both in silico simulation based on the crystal structure of the proteins and NMR titration studies for observation of both chemical sift changes and PRE effects can strongly support the elucidation of the crucial mechanism of PPI inhibitions by a small molecule.

Acknowledgements

We thank Dr. Naoki Goshima, Dr. Shun-ichiro Iemura, and Dr. Satoshi Karasawa for helpful discussion. The cDNA encoding PAC3 was kindly provided by Dr. Keiji Tanaka (The Tokyo Metropolitan Institute of Medical Science, Tokyo, Japan). We thank Eiji Kurimoto (NCU), Kenta Okamoto (NCU), and Olivier Serve (IMS) for their contributions at the early stage of this study. We also thank Kiyomi Senda, Kumiko Hattori (NCU), and Yukiko Isono (IMS) for their help in the preparation of isotopically labeled protein and Shionogi & Co., Ltd. for providing the initial samples of natural thielocins. This study was supported by a grant from the New Energy and Industrial Technology Development Organization (NEDO) of Japan, in part by the Japan Society for the Promotion of Science (JSPS)/ the Ministry of Education, Culture, Sports, Science and Technology (MEXT) Grants-in-Aid for Scientific Research (24657113 and 25102008), MEXT Targeted Proteins Research Program and Nanotechnology Platform Program. We thank JSPS also for support from the GCOE program (Tohoku Univ).

Notes and references

[a] *Graduate School of Pharmaceutical Sciences, Tohoku University, 6-3 Aza-aoba, Aramaki, Aoba-ku, Sendai 980-8578, Japan. Fax: (+81) 22 795 6865; E-mail: doi_taka@mail.pharm.tohoku.ac.jp*
[b] *National Institute of Advanced Industrial Science and Technology (AIST), 2-4-7 Aomi, Koto-ku, Tokyo 135-0064, Japan.*
[c] *Biomedicinal Information Research Center (BIRC), Japan Biological Informatics Consortium (JBIC), 2-4-7 Aomi, Koto-ku, Tokyo 135-0064, Japan.*
[d] *Okazaki Institute for Integrative Bioscience and Institute for Molecular Science, National Institutes of Natural Sciences, 5-1 Higashiyama, Myodaiji, Okazaki, Aichi 444-8787, Japan.*
[e] *Graduate School of Pharmaceutical Sciences, Nagoya City University, 3-1 Tanabe-dori, Mizuho-ku, Nagoya 467-8603, Japan.*
[f] *Computational Biology Research Center (CBRC), National Institute of Advanced Industrial Science and Technology (AIST), 2-4-7 Aomi, Koto-ku, Tokyo 135-0064, Japan.*

† Electronic Supplementary Information (ESI) available: Synthetic protocols and characterization data, methods for docking study and molecular dynamics simulation, protein expression and purification, and NMR titration, and ^{1}H and ^{13}C NMR spectra of **1**, **2b**, **3**, **4**, and **7**–**19**. See DOI: 10.1039/b000000x/

1 H. Yin, A. D. Hamilton, *Angew. Chem. Int. Ed.,* 2005, **44**, 4130.
2 T. Clackson, J. A. Wells, *Science,* 1995, **267**, 383.
3 T. Clackson, M. H. Ultsch, J. A. Wells, A. M. de Vos, *J. Mol. Biol.,* 1998, **277**, 1111.
4 J. A. Wells, C. L. McClendon, *Nature,* **2007**, *450*, 1001.
5 K. McMillan, M. Adler, D. S. Auld, J. J. Baldwin, E. Blasko, L. J. Browne, D. Chelsky, D. Davey, R. E. Dolle, K. A. Eagen, S. Erickson, R. I. Feldman, C. B. Glaser, C. Mallari, M. M. Morrissey, M. H. Ohlmeyer, G. Pan, J. F. Parkinson, G. B. Phillips, M. A. Polokoff, N. H. Sigal, R. Vergona, M. Whitlow, T. A. Young, J. J. Devlin, *Proc. Natl. Acad. Sci. U.S.A.,* 2000, **97**, 1506.
6 O. Keskin, A. Gursoy, B. Ma, R. Nussinov, *Chem. Rev.,* 2008, **108**, 1225.
7 A. J. Wilson, *Chem. Soc. Rev.,* 2009, **38**, 3289.
8 G. Zinzalla, D. E. Thurston, *Future Med. Chem.,* 2009, **1**, 65.
9 O. Sperandio, C. H. Reynés, A.-C. Champroux, B. O. Villoutreix, *Drug Discov. Today* **2010**, *15*, 220; A. Mullard, *Nat. Rev. Drug Discov.,* 2012, **11**, 173.
10 J. Hashimoto, T. Watanabe, T. Seki, S. Karasawa, M. Izumikawa, T. Seki, S. Iemura, T. Natsume N. Nomura, N. Goshima, A. Miyawaki, M. Takagi, K. Shin-ya, *J. Biomol. Screen.,* 2009, **14**, 970.
11 Y. Hirano, H. Hayashi, S. Iemura, K. B. Hendil, S. Niwa, T. Kishimoto, M. Kasahara, T. Natsume, K. Tanaka, S. Murata, *Mol. Cell,* 2006, **24**, 977.
12 H. Yashiroda, T. Mizushima, K. Okamoto, T. Kameyama, H. Hayashi, T. Kishimoto, S. Niwa, M. Kasahara, E. Kurimoto, E. Sakata, K. Takagi, A. Suzuki, Y. Hirano, S. Murata, K. Kato, T. Yamane, K. Tanaka, *Nat. Struct. Mol. Biol.,* 2008, **15**, 228.
13 Y. Hirano, K. B. Hendil, H. Yashiroda, S. Iemura, R. Nagane, Y. Hioki, T. Natsume, K. Tanaka, S. Murata, *Nature,* 2005, **437**, 1381.
14 B. Le Tallec, M. B. Barrault, R. Courbeyrette, R. Guerois, M. C. Marsolier-Kergoat, A. Peyroche, *Mol. Cell,* 2007, **27**, 660.
15 A. R. Kusmierczyk, M. J. Kunjappu, M. Funakoshi, M. Hochstrasser, *Nat. Struct. Mol. Biol.,* 2008, **15**, 237.
16 P. C. Ramos, R. J. Dohmen, *Structure,* 2008, **16**, 1296.
17 A. C. Matias, P. C. Ramos, R. J. Dohmen, R. J. *Biochem. Soc. Trans.,* 2010, **38**, 29.
18 T. Yoshida, K. Inoue, H. Arita, S. Matsutani, Y. Kawamura, JP 04117346, 1992 [*Chem. Abstr.,* 1992, **117**, 210731]; S. Matsutani, R. Sakazaki, H. Hinoo, Y. Terui, K. Tanaka, K. Matsumoto, T. Yoshida, *Symposium on the chemistry of natural products* (Japan), 1992, **34**, 142; K. Tanaka, S. Matsutani, A. Kanda, T. Kato, T. Yoshida, *J. Antibiot.,* 1994, **47**, 631.
19 K. Matsumoto, K. Tanaka, S. Matsutani, R. Sakazaki, H. Hindo, N. Uotani, T. Tanimoto, Y. Kawamura, S. Nakamoto, T. Yoshida, *J. Antibiot.,* 1995, **48**, 106.
20 M. Izumikawa, J. Hashimoto, T. Hirokawa, S. Sugimoto, T. Kato, M. Takagi, K. Shin-ya, *J. Nat. Prod.,* 2010, **73**, 628.
21 R. A. Friesner, J. L. Banks, R. B. Murphy, T. A. Halgren, J. J. Klicic, D. T. Mainz, M. P. Repasky, E. H. Knoll, M. Shelly, J. K. Perry, D. E. Shaw, P. Francis, P. S. Shenkin, *J. Med. Chem.,* 2004, **47**, 1739.
22 Y. Génisson, P. C. Tyler, R. N. Young, *J. Am. Chem. Soc.,* 1994, **116**, 759.
23 Y. Génisson, P. C. Tyler, R. G. Ball, R. N. Young, *J. Am. Chem. Soc.,* 2001, **123**, 11381.
24 Y. Génisson, R. N. Young, *Tetrahedron Lett.,* 1994, **35**, 7747.
25 I. Teshirogi, S. Matsutani, K. Shirahase, Y. Fujii, T. Yoshida, K. Tanaka, M. Ohtani, *J. Med. Chem.,* 1996, **39**, 5183.
26 J. B. Hendrickson, M. V. J. Ramsay, T. R. Kelly, *J. Am. Chem. Soc.,* 1972, **94**, 6834.
27 T. Sala, M. V. Sargent, *J. Chem. Soc. Perkin Trans. 1,* 1981, 855.
28 T. Sala, M. V. Sargent, *J. Chem. Soc. Perkin Trans. 1,* 1981, 877.

29 J. M. Keith, *Tetrahedron Lett.,* 2004, **45**, 2739.
30 H. Tanaka, H. Miyoshi, Y.-C. Chuang, Y. Ando, T. Takahashi, *Agnew. Chem. Int. Ed.,* 2007, **46**, 5934.
31 C. T. West, S. J. Donnelly, D. A. Kooistra, M. P. Doyle, *J. Org. Chem.,* 1973, **38**, 2675.
32 R. Gedye, F. Smith, K. Westway, H. Ali, L. Baldisera, L. Laberge, J. Rousell, *Tetrahedron Lett.,* 1986, **27**, 279.
33 C. O. Kappe, D. Dallinger, *Mol Divers.,* 2009, **13**, 71.
34 H. L. Goering, T. Rubin, M. S. Newman, *J. Am. Chem. Soc.,* 1954, **76**, 787.
35 L. R. C. Barclay, N. D. Hall, G. A. Cooke, *Can. J. Chem.,* 1962, **40**, 1981.
36 R. C. Parish, L. M. Stock, *J. Org. Chem.,* 1965, **30**, 927.
37 A. Vilsmeier, A. Haack, *Ber. Dtsch. Chem. Ges.,* 1927, **60**, 119.
38 W. E. Smith, *J. Org. Chem.,* 1972, **37**, 3972.
39 K. Reimer, F. Tiemann, *Ber.,* 1876, **9**, 824; K. Reimer, F. Tiemann, *Ber.,* 1876, **9**, 1268; K. Reimer, F. Tiemann, *Ber.,* 1876, **9**, 1285.
40 A. Rieche, H. Gross, E. Höft, *Chem. Ber.-Recl.,* 1960, **93**, 88.
41 K. Ohsawa, M. Yoshida, T. Doi, *J. Org. Chem.,* 2013, **78**, 3438.
42 B. O. Lindgren, T. Nilsson, *Acta Chem. Scand.,* 1973, **27**, 888; G. A. Kraus, M. J. Taschner, *J. Org. Chem.,* 1980, **45**, 1174; B. S. Bal, W. E. Childers, Jr., H. W. Pinnick, *Tetrahedron,* 1981, **37**, 2091.
43 J. Iwahara, G. M. Clore, *Nature*, 2006, **440**, 1227.
44 M. Yagi-Utsumi, T. Kameda, Y. Yamaguchi, K. Kato, *FEBS Lett.*, 2010, **584**, 831.
45 Molecular Operating Environment (MOE), ver. 2012, Chemical Computing Group Inc., 1010 Sherbrooke Street West, Suite 910, Montreal, Quebec, Canada H3A 2R7.
46 T. S. Rush III, J. A. Grant, K. Mosyak, A. Nicholls, *J. Med. Chem.,* 2005, **48**, 1489.
47 A. G. Cochran, *Chem. Biol.,* 2000, **7**, R85.
48 M. M. He, A. S. Smith, J. D. Oslob, W. M. Flanagan, A. C. Braisted, A. Whitty, M. T. Cancilla, J. Wang, A. A. Lugovskoy, J. C. Yoburn, A. D. Fung, G. Farrington, J. K. Eldredge, E. S. Day, L. A. Cruz, T. G. Cachero, S. K. Miller, J. E. Friedman, I. C. Choong, B. C. Cunningham, *Science,* 2005, **310**, 1022.
49 M. D. Wendt, C. Sun, A. Kunzer, D. Sauer, K. Sarris, E. Hoff, L. Yu, D. G. Nettesheim, J. Chen, S. Jin, K. M. Comess, Y. Fan, S. N. Anderson, B. Isaac, E. T. Olejniczak, P. J. Hajduk, S. H. Rosenberg, S. W. Elmore, *Bioorg. Med. Chem. Lett.,* 2007, **17**, 3122.